行政院國家科學委員會專題研究計畫　期中進度報告

利用化學控制合成新穎電子/離子作用氧化物及其特性分析

(1/3)

計畫類別：個別型計畫
計畫編號：NSC91-2113-M-002-044-
執行期間：91 年 08 月 01 日至 92 年 07 月 31 日
執行單位：國立臺灣大學化學系暨研究所

計畫主持人：劉如熹

計畫參與人員：詹丁山、王健源、張嵩駿、紀喨勝、林欣瑋、陳浩銘、周大為、林益山

報告類型：精簡報告
報告附件：出席國際會議研究心得報告及發表論文
處理方式：本計畫可公開查詢

中　華　民　國 92 年 5 月 29 日

行政院國家科學委員會補助專題研究計畫成果報告

※※※※※※※※※※※※※※※※※※※※※※※※※

※

※

※ 利用化學控制合成新穎電子/離子作用氧化物

※

※ 及其特性分析(1/3)

※

※※※※※※※※※※※※※※※※※※※※※※※※※

計畫類別：☑個別型計畫 □整合型計畫

計畫編號：NSC 91-2113-M-002-044

執行期間：91 年 8 月 1 日 至 92 年 7 月 31 日

計畫主持人：劉如熹

本成果報告包括以下應繳交之附件：

□赴國外出差或研習心得報告一份

□赴大陸地區出差或研習心得報告一份

☑出席國際學術會議心得報告及發表之論文各一份

□國際合作研究計畫國外研究報告書一份

執行單位：台灣大學化學系

中　華　民　國　九十二年　五　月二十七日

行政院國家科學委員會專題研究計畫成果報告

利用化學控制合成新穎電子/離子作用氧化物及其特性分析

(1/3)

Synthesis by Chemical Control and Characterization of New Electronic/Ionic Oxides

計畫編號：NSC 91-2113-M-002-044

執行期限：91 年 8 月 1 日至 92 年 7 月 31 日

主持人：劉如熹 教授（台灣大學化學系）

計畫參與人員：詹丁山、王健源、張嵩駿、紀喨勝、林欣瑋、陳浩銘、周大為、林益山（台灣大學化學系）

一、中文摘要

隨科技之進步，資訊產業之發展也日新月異，資訊產品愈來愈多樣化，且持續有各式各樣之紀錄媒體相繼研發中，藉以滿足人類對大量資料儲存與紀錄上之需求。自 1995 年具穿隧式磁電阻 (tunneling magnetoresistance; TMR)效應之材料得到突破性之進展，短短幾年內，其磁性感應度即提高一倍以上。TMR 於室溫時之 25~50 % 磁電阻值，遠遠高於傳統之巨磁電阻 (giant magnetoresistance; GMR)材料(室溫~ 10 %)，使其對於各式紀錄媒體而言更具發展潛力。有鑑於此，本研究乃探討於 Sr_2FeMoO_6 ($Sr_2BB'O_6$)雙層鈣鈦礦化合物中，固定鹼土族鍶離子，藉由不同 3*d*、4*d* 與 5*d* 之過渡金屬離子，取代 B 或 B′之位置。計合成以 $3d^5$(Fe)為主之 Sr_2FeMoO_6 (Fe^{3+}：Mo^{5+} ⇔ $3d^5$：$4d^1$)與 Sr_2FeWO_6 (Fe^{3+}：W^{5+} ⇔ $3d^5$：$5d^1$)系統，進而研究其晶體結構、磁性、電性等性質，以期開發最佳配置且特性卓越之穿隧磁電阻材料。

關鍵詞：穿隧式磁電阻、巨磁電阻、雙層鈣鈦礦、Sr_2FeMoO_6、Sr_2FeWO_6.

一、Abstract

By the technological improvement, the information development is changing with the passing day and various several mediums are keeping researching to satisfy the request of data's storage and recordation. Since 1995 materials of TMR (tunneling magnetoresistance) effect were improved evidently, in few years it's magnetic induction rose double. TMR materials show much higher MR% (about 25~50%) than traditional GMR materials (about 10%) under room temperature, so it is considered to apply to MR sensor of the magnetic recording industry. Accordingly, in this research the Sr_2FeMoO_6 ($Sr_2BB'O_6$) double perovskites compounds were fabricated by keeping the stoichiometry of the alkaline earth strontium ion and displacing the position of B or B′ with different 3*d*, 4*d* and 5*d* transition metals. Therefore, based syatems of $3d^5$(Fe) systems of Sr_2FeMoO_6 (Fe^{3+}：Mo^{5+} ⇔ $3d^5$：$4d^1$) and Sr_2FeWO_6 (Fe^{3+}:W^{3+} ⇔ $3d^5$:$5d^1$) systems have been

synthesized. Moreover, their crystal structures, magnetic and electrical properties have been studied which may lead to develop the optimal composition and excellent properties of the new TMR materials.

Keywords: tunneling magnetoresistance (TMR)、giant magnetoresistance (GMR)、double perovskites、Sr_2FeMoO_6、Sr_2FeWO_6

二、緣由與目的

In ordered double perovskites denoted as $A_2BB O_6$ (where A = alkaline-earth or rare-earth ion), the transition metal sites are occupied alternately by different cations B and B . It is known that the differences in the valence and size between the B and B cations in double perovskites type compounds are crucial to controlling the physical properties.[1-2] Among them, Sr_2FeMoO_6 have been known as potential magnetoresistance materials, which show large low-field tunneling magnetoresistance (TMR) at room temperature (RT).[3] The magnetic structure of Sr_2FeMoO_6 was attributed to an ordered arrangement of parallel Fe^{3+} ($3d^5$, S = 5/2) magnetic moments, antiferromagnetically coupled with Mo^{5+} ($4d^1$, S = 1/2) spins. Since Fe^{3+} is in the high spin state, its d orbitals are split into spin up and spin down states. Sleight et al.[4] proposed that if the spin down $3d$ orbitals of Fe have similar energy to the $4d$ orbitals of Mo, they can form a narrow band and provide the conduction mechanism. The band calculations, which show a mixing of the spin-down O $2p$, Fe $3d$ and Mo $4d$ bands at the Fermi level supported this mechanism.[3,5-6] Other Fe-based ordered double perovskites A_2FeMO_6 (A = Ba, Sr, Ca; M= Mo, Re) have also been reported to have half-metallic nature and high Tc .[7-13]

On the other hand, recently, the further study to figure out some effects of Fe/Mo disorder on magnetic and electrical properties in Sr_2FeMoO_6.[14,15] For ordered state, the Fe^{3+} and Mo^{5+} ions antiferromagnetically coupled and give rise to ferromagnetic metal with saturated magnetization Ms = 4 ì B. However, most of the experiments data showed a reduced Ms. This fact seems to be related to antisite defects, where some of the Fe and Mo ions interchange their crystallographic positions. The actual degree of Fe/Mo order depends on synthesis conditions. As a rule of thumb, increased order may be obtained with increased synthesis temperature or treatment time.[16,17]

In relation to the electronic configurations of the Sr_2FeMoO_6, the average valence for Fe was also been found to be intermediate between high spin configurations values of Fe^{2+} and Fe^{3+} from MÖssbauer spectroscopy studies.[8,18,19] This suggests that both electronic configurations with Fe^{2+} and Fe^{3+} must be considered as degenerate, with the final state being a combination of both configurations. Conversely, Sr_2FeWO_6 is know as an antiferromagnetic insulator with T_N of 16-37 K, where Fe^{2+} ions is in the high-spin state (S = 2), and W^{6+} ion ($5d^0$) is in the non-magnetic state.[20-22] This would give rise to a complete localization of the valence electrons, explaining the decrease in conductivity. Therefore, the fundamental question is why the W case so different from the Mo case despite the fact that W is $5d$ analogue of $4d$ Mo in the row of the Periodic Table?

In this research we report the synthesis and characterization of the Sr_2FeMO_6 (M = Mo, W) samples with particular focus on the effect of the variation of B -site transition metal on the physical properties. We will show that the stronger $2p$(O)-$4d$(Mo) hybridization compared with the $2p$(O)-$5d$(W) hybridization is the main source of the difference between Sr_2FeMoO_6 and Sr_2FeWO_6.

三、研究方法

Sample Preparation. The samples of Sr_2FeMO_6 (M = Mo, W) were prepared by solid state reaction. Stoichiometric mixtures of high purity oxides $SrCO_3$, Fe_2O_3 or MoO_3 and WO_3 were calcined at 800 °C for 12 h in air. The obtained powders were ground and pressed into pellets (15 mm in diameter and 3 mm in thickness). The pellets of Sr_2FeMoO_6 were then sintered at 1000 °C for 38 h in a 5 % H_2 / N_2 gas mixture. However, the pellets of Sr_2FeWO_6 were sintered at 1200 °C for 18 h in a 5 % H_2 / N_2 gas mixture.

Characterization. X-ray diffraction (XRD) measurements were carried out on a SCINTAG (X1) diffractmeter (Cu K~ radiation, ª = 1.5406 Å) at 40 kV and 30 mA. The GSAS program[23] was used for the Rietveld refinements in order to obtain information on the crystal structures of Sr_2FeMO_6 (M = Mo, W). A pseudo-Voigt function was chosen to generate the line shape of the diffraction peaks. In the final runs, the positional coordinates, isotropic thermal factors, and anti-site disorder of Fe、Mo and W atoms were refined. Scanning electron micrographs (SEMs) were measured at room temperature by a Philips XL30 SEM equipped with a field emission gun at 15 kV. Electron diffraction (ED) and high resolution transmission electron microscopy (HRTEM) were carried out using a JEOL 4000EX electron microscope operated at 400 kV. Image simulation was made using CaRIne software. The samples for microscopic measurement were dispersed in alcohol before being transferred to the carbon coated copper grids. The resistively measurements at zero field [(ñ(T))] and under a magnetic field [(ñ(H))] were performed with a Quantum Design PPMS (physical properties measurements system), using the conventional four-probe technique, under magnetic fields up to 3 T. Magnetization measurements were performed on a SQUID magnetometer from 0 to 350 K in field-cooled (FC) and Zero-field-cooled (ZFC) modes.

X-ray Absorption Measurements. X-ray absorption near edge structure (XANES) measurements at Fe-L_{23} were performed at the national synchrotron radiation research center (NSRRC) in Hsinchu, Taiwan with an electron beam

energy of 1.5 GeV and a maximum stored current of 240 mA. All the measurements were performed at room temperature. The XANES measurements at the Fe-L_{23} edge were performed at the 6-m high-energy spherical grating monochromatic (HSGM) beamline BL20A. The sample were in powder form, attached on conducting tape, and then put into an ultrahigh vacuum chamber (10^{-9} Torr) in order to avoid surface contamination. The spectra were recorded by measuring the sample current. The incident photon flux (I_0) was monitored simultaneously by using a Ni mesh located after the exit slit of the monochromatic beam. The reproducibility of the adsorption spectra of the same sample in different experimental runs was found to be extremely good.

Band structure calculations. Band structures of tetragonal (Sr_2FeMoO_6) and orthorhombic (Sr_2FeWO_6) were calculated using the all-electron full-potential theory linear augmented plane wave (FLAPW) method.[24] These calculations were based on first-principles density functional theory (DFT) with the generalized gradient approximation (GGA) to the exchange-correlation potential. Fe 4*s*4*p*3*d*, Mo 5*s*5*p*4*d*, W 6*s*6*p*5*d*, O 2*s*2*p*, and Sr 5*s*5*p*5*d* were treated as band states. The shallow Fe:3*s*3*p*, Mo:4*s*4*p*, W:5*s*5*p*, and Sr:4*s*4*p* orbitals were also treated as band states by using the so-called local orbitals. A large number (~120/atom) of augmented plane waves were used. The wave function, charge densities, and potentials were expanded in terms of the spherical harmonics inside the muffin-tin spheres with L_{max} = 10, 6 and 6, respectively.

四、結果與討論

The powder XRD patterns of the Sr_2FeMO_6 (M = Mo, W) samples are shown in Figure 1. Each composition of these samples is of single phase. For the samples with Sr_2FeMoO_6 and Sr_2FeWO_6 all the peaks in each pattern can be indexed on the basis of a tetragonal (space group: *I*4/*m*) and orthorhombic unit cell (space group: *Immm*), respectively. Moreover, the concept of the tolerance factor can be adapted to double perovskites as well. In general, for double perovskites, with mixed A-site AA´BB´O_6, the tolerance factor (t_{factor}) is defined: [25,26]

$$t = \frac{\frac{r_A + r_{A'}}{2} + r_O}{\sqrt{2}(\frac{r_B + r_{B'}}{2} + r_O)} \qquad (1)$$

In which r_A, $r_{A'}$, r_B, $r_{B'}$ and r_O are the ionic radii of the respective ions. The t_{factor} = 1 for the compound with an ideal cubic perovskite structure. If t_{factor} < 1, the perovskite structure is likely to be unstable. Therefore, the t_{factor} decreased (from 0.990 for Sr_2FeMoO_6 to 0.988 for Sr_2FeWO_6) while gave rise to unstable the structure and induced structure changes from tetragonal to orthorhombic unit cell at RT. Figures 2 (a) and (b) display the observed and calculated X-ray powder diffraction profiles at 300 K of Sr_2FeMO_6 (M = Mo, W) samples, respectively. All the observed peaks can be fitted with the reflection conditions of the space groups *I*4/*m* for Sr_2FeMoO_6 and *Immm* for Sr_2FeWO_6, respectively. The refined occupancies of the Fe and Mo(W) sites shows that the ratios of Fe/Mo and Fe/W anti-site disorder are around 14% and 0.1% , respectively. Sánchez et al.[17] proposed that the actual degree of order depends mainly on synthesis conditions. Therefore, an increase in order in Sr_2FeWO_6 may be obtained with increasing the synthesis temperature. The lattice parameters (*a* and *c*) and cell volume of the Sr_2FeWO_6 sample are significantly larger than that of the Sr_2FeMoO_6 sample which is due to the radius of the W^{5+} ions (0.62 Å) is larger than that of the Mo^{5+} (0.61 Å) ions.[27] Furthermore, the Fe-O distances of Sr_2FeWO_6 (2.059 Å) are large than those in Sr_2FeMoO_6 (1.969 Å). Additionally, W-O distance (1.920 Å) is shorter than those in Mo-O distance (1.973 Å). Based on the unit cell data reported by Sánchez et al.[17] The ordered sample FeO_6 octahedral is significantly larger (expanded) than MoO_6 octahedral. This observation is coherent with the large ionic size of Fe^{3+} vs Mo^{5+}.[27] For the disordered sample the Fe-O and Mo-O bond lengths are more similar, as expected for the high degree of antisite disordering. Our results show the more disordered sample Sr_2FeMoO_6 (14% anti-site disorder) have similar Fe-O (1.969 Å)and Mo-O (1.973 Å) bond lengths. Moreover, the more ordered sample Sr_2FeWO_6 (0.1% anti-site disorder) have significantly larger FeO_6 octahedral more than WO_6 octahedral. The results were consistent with the published results.[17]

The morphology of Sr_2FeMO_6 (M = Mo, W) with (a) Sr_2FeMoO_6 and (b) Sr_2FeWO_6 are observed with a SEM as shown in Figure 3. Sr_2FeWO_6 microcrystals (1200 ℃) are distribution high homogeneity morn than that of Sr_2FeMoO_6 (1000 ℃). This seems to indicate that the increasing the synthesis temperature can help the grain growth during the sintering process. It also shows the shape and size of Sr_2FeMO_6 (M = Mo, W) about the range 2~3 ì m.

Figures 4 (a) and 4 (b) show a typical ED pattern and HRTEM lattice image, respectively, recorded along the [100] zone-axis direction of Sr_2FeWO_6. The simulated pattern along zone axis [100] is shown in Figure 5 (c). The cell symmetry obtained by ED was identified by the observation only of *h k l*; *h* + *k* + *l* = 2 *n* reflections indicating *I*-centering of the unit cell which is consistent with the XRD refinement result.

The temperature dependence of high-field (H = 5 T) magnetization of Sr_2FeMO_6 (M = Mo, W) was shown in Figure 5 (a). Magnetic measurements indicate an antiferromagnetic ordering for Sr_2FeWO_6 and ferromagnetic ordering for Sr_2FeMoO_6. Figure 5 (b) shows magnetic hysteretic curves recorded of Sr_2FeMO_6 (M = Mo, W) at T = 5 K. For the reason clarity, we only display the region of 1 T ≥ H ≥ -1 T. The magnetization curves measured at 5 K show no appreciable hysteresis for Sr_2FeWO_6. Moreover, it also shows the hysteresis loop below 1 T for Sr_2FeMoO_6 in Figure 5 (b), consistent with the ferromagnetic behavior mentioned above.

In the case of Sr_2FeWO_6, this corresponds to the

antiferromagnetic transition (T_N), and T_N ~35 K (Figure 6) in good agreement with a report of 37 K.[10] As shown in Figure 6, the Curie-Weiss plot for Sr_2FeWO_6 gives Curie constant C = 6.08 and Weiss temperature $\dot{e}$ = -32.6 K. The small and negative value of $\dot{e}$ suggests that although there exists both weak ferromagnetic and antiferromagnetic interactions at low temperature. The antiferromagnetic interaction dominates over the weak ferromagnetic one. This point will be discussed later in detail.

Figure 7 shows the (a) zero-field cooled (ZFC) and (b) field cooled (FC) magnetic susceptibility (÷) vs. temperature of Sr_2FeWO_6 measured with the applied field H =0.1, 0.5, 1, 3 and 5 T, respectively. The magnetic interactions are predominantly antiferromagnetic. At ~25 K there is a smaller feature which likely the result of a spin-reordering process on the magnetic sublattice. Furthermore, the presence of a spontaneous spin-reordering process is further emphasized by the magnetic measurement exhibited by the ZFC and FC curves; below the transition temperature (25 K), the ZFC and FC curves show large deviations. With increasing field, the transition is gradually masked. This seems to indicate that the presence of a weak ferromagnetic moment which can be ascribed to moment canting on the sublattices. Magnetic hysteresis curves obtained at 5 K are shown in Figure 6 (b) demonstrates the existence of a weak ferromagnetic response additionally indicating that the predominant character of the response is linear in field. This behavior was consistent with the published results.[28,29]

The transport properties of Sr_2FeMO_6 (M = Mo, W) samples are illustrated in Figure 8. Both ñ(H = 0T), ñ(H = 1 T) and ñ(H = 3T) show a half-metallic behavior over the whole temperature range down to 5 K for Sr_2FeMoO_6 and an insulator behavior over the whole temperature range down to around 170 K for Sr_2FeWO_6. Plots of magnetoresistance (MR) against temperature for Sr_2FeMO_6 (M = Mo, W) are also given in the inset of Fig. 8. The MR ratio is define by MR (T,H) = [ñ (T,H = 0) - ñ (T,H = 3 T)]/ ñ (T,H = 3 T)] where H denotes the external field. The large MR ratio of ~22% (H = 3 T) at room temperature (RT) was observed in the Sr_2FeWO_6 compound. However, the Sr_2FeMoO_6 compound did not show any significant MR even at high fields and RT (MR ~ 1% ; H = 3 T and 300 K).

Information about the effective oxidation states of Fe and the local structural distortions around these ions is provided by X-ray absorption spectroscopic (XAS) investigations. Specifically the chemical shift of an atomic absorption edge to high energy, with increasing formal oxidation state of that atom, is the simplest and most commonly used XAS valence indicator. Figure 9 shows the Fe $L_{2,3}$-edge XANES spectra of Sr_2FeMoO_6 and Sr_2FeWO_6 along with the FeO, Fe_3O_4 and Fe_2O_3 standards. The main spectral features of the $L_{2,3}$ edge of Fe originate from dipole transitions from the core Fe 2*p* level to the empty Fe 3*d* states.[30,31] The spectra show two broad multiplet structures separated by spin–orbit splitting of Fe $2p_{3/2}$ (L_3 edge; 705 ~ 715 eV) and Fe $2p_{1/2}$ (L_2 edge; 715 ~ 725 eV). Both the edges, L_3 and L_2, are further divided into two peaks. The splitting and intensity ratio between the two peaks is determined by the interplay of crystal-field effects and electronic interactions. The L_3 absorption edge of Fe^{II} species in an octahedral crystal field typically exhibits a main peak at a lower energy (~708 eV), followed by a weaker peak or a shoulder at a higher energy (~710 eV). Based on the chemical shift, both the Sr_2FeMoO_6 and Sr_2FeWO_6 of Fe valence is much greater than 2+ but less than 3+. The average valence for Fe has also been found to be intermediate between high-spin configurations values of Fe^{2+} and Fe^{3+} from MÖssbauer spectroscopy studies.[8,32] Moreover, the Fe valence of Sr_2FeMoO_6 is slightly lower that that of Sr_2FeWO_6 as compared to the relative intensity at the energy of 708 eV and 710 eV, respectively.[13] This phenomenon may be correlated to the anti-site effect of the titled compounds.

To discuss the different transport properties between the Sr_2FeMO_6 (M = Mo, W) samples, we use the full-potential augmented plane-wave (FLAPW) method to do the band structure calculations. The calculations were based on the Rietveld refined models of $Sr_2FeMoO_6$with the tetragonal unit cell and Sr_2FeWO_6 with the orthorhombic unit cell. The density of states obtained by this calculation is shown in Figure 10 (a) for Sr_2FeMoO_6 and (b)(c)for Sr_2FeWO_6. The predicted electronic features for Sr_2FeMoO_6 and Sr_2FeWO_6resembles those calculated by Kobayashi et al.[3] and Fang et al.[6] Based on the above descriptions, the fundamental question is why the W case so different from the Mo case despite the fact that W is 5*d* analogue of Mo in the row of the Periodic Table? Fang et al.[6] proposed that the *p-d* hybridization between oxygen and M (Mo, W) to the main source of this different. Because the 5*d* orbital of W is more extended than the 4*d* orbital of Mo, the stronger 2*p*(O)-5*d*(W) hybridization pushes the 5*d* band, which is the *p-d* antibonding state, higher in energy. Therefore the Sr_2FeWO_6 band gap opens up and the electron transfer will not occur. Our band structure calculations as shown in Figure 10 are consistent with the published results[6] and show that the *p-d* bonding counter part in the energy position of the spin-up t_{2g} bands is clearly deeper for Sr_2FeWO_6 than that of Sr_2FeMoO_6.

五、結論

In order to investigated the interaction among 3*d*(Fe)、4*d*(Mo) and 5*d*(W) orbitals of transition metal ions via oxygen ions. The crystal structure, magnetic and magnetotransport properties of B -site transition metal Sr_2FeMO_6 (M = Mo, W) with double perovskites structure have been investigated systematically. Powder X-ray diffraction analyses revealed that Sr_2FeMoO_6 and Sr_2FeWO_6 have the tetragonal cell (space group: *I4/m*) and the orthorhombic cell (space group: *Immm*), respectively.

The Curie-Weiss fit for Sr_2FeWO_6 gives Curie constant C = 6.08 and Weiss temperature θ = -32.6 K. The small and negative value of θ suggests that although there exists both weak ferromagnetic and antiferromagnetic interactions at low temperature. The properties of these two compounds are summarized as follows: Sr_2FeMoO_6 - half-metallic and ferromagnetic; Sr_2FeWO_6 - insulator and antiferromagnetic. The changes observed by physical measurements are supported by FLAPW band structure calculations to explain the interaction between the 3*d*(Fe)、4*d*(Mo) and 5*d*(W) orbitals of transition metal ions and oxygen ions. The *p-d* bonding counter part in the energy position of the spin-up t_{2g} bands is deeper for SFWO than that of SFMO.

六、計畫成果自評

We have reached the goals of the research plan, some part of the results have already publicized or in scientific journals [13,32,33].

七、參考文獻

[1] Galasso, F. *Inorg. Chem.* 1963, **2**, 482.

[2] Nakamura, T.; Choy, J. H. *J. Solid State Chem.* 1977, **20**, 233.

[1]

[3] Kobayashi, K. -I.; Kimura, T.; Sawada, H,; Terakura, K.; Tokura, Y. *Nature*. 1998, **395**, 677.

[4] Sleight, A. W.; Weiher, J. F. *J. Phys. Chem. Solids*. 1972, **33**, 679.

[5] Kim, T. H.; Uehara, M.; Cheong, S. W.; Lee, S. *Appl. Phys. Lett*. 1999, **74**, 1737.

[6] Fang, Z.; Terakura, K.; Kanamoru, J. *Phys. Rev. B* 2001, **63**, 180407.

(1)[7] Maignan, A.; Raveau, B.; Martin, C.; Hervieu, M. *J. Solid State Chem.* 1999, **59**, 11159.

(8)[8] Alonso, J. A.; Casais, M. T.; Martínze-Lope, M. J.; Velasco, P.; Muñoz, A.; Fernández-Díaz, M. T. *Chem. Mater*. 2000, **12**, 161.

(8)[9] Borges, R. P.; Thomas, R. M.; Cullinan, C.; Coey, J. M. D.; Suryanarayan, R.; Ben-Dor, L.; Pinsard-Gaudart, L.; Revcolevschi, A. *J. Phys.: Condens. Matte*r. 1999, **11**, L445.

(10)[10] Ritter, C.; Ibarra, M. R.; Morellón, L.; Blasco, J.; García, J.; De Teresa, J. M. *J. Phys.: Condens. Matte*r. 2000, **12**, 8295.

(11)[11] Prellier, W.; Smolyaninova, W.; Bisbas, A.; Galley, C.; Greene, R. L.; Ramesha, K.; Gopalakrishnan. J. *J. Phys.: Condens. Matter*. 2000, **12**, 965.

[12] Kobayashi, K. -I.; Kimura, T.; Sawada, H,; Terakura, K.; Tokura, Y. *Phys. Rev. B* 1999, **59**, 11159.

[13] Chan, T. S.; Liu, R. S.; Guo, G. Y.; Hu, S. F.; Lin, J. G.; Chen, J. M.; Attfield, J. P. *Chem. Mater.* 2003, **15**, 425.

[14] Tomioka, Y.; Okuda, T.; Kumai, R.; Kobayashi, K. -I.; Tokura, Y. *Phys. Rev. B* 2000, **61**, 422.

(1)[15] Balcells, L.; Navarro, J.; Bibes, M.; Roig, A.; Martinez, B.; Fontcuberta, J. *Appl. Phys. Lett.* 2001, **78**, 781.

(1)[16] Woodward, P.; Hoffmann, R. D.; Sleight, A. W. *J. Mater. Res.* 1994, **9**, 2118.

[17] Sánchez, D.; Alonso, J. A.; García-Hernández, M.; Martínze-Lope, M. J.; Martínez, J. L. *Phys. Rev. B* 2002, **65**, 104426.

[18] Woodward, P. M. *Acta Crystallogr., Sect.* B 1997, **53**, 32.

[19] Viola, M. C.; Martínze-Lope, M. J.; Alonso, J. A.; Velasco, P.; Martínze, J. L.; Pedregosa, J. C.; Carbonio, R. E.; Fernández-Díaz, M. T. *Chem. Mater*. 2002, **14**, 812.

[20] Blasse, G. *Philips Res. Rep*. 1965, **621**, 422.

[21] Nakagawa, T.; Yoshikawa, K.; Nomura, S. *J. Phys. Soc. Japan*. 1969, **27**, 880.

[22] Kawanaka, H.; Hase, I.; Toyama, S.; Nishihara, Y. *J. Phys. Soc. Japan*. **1999**, *68*, 2890.

(24)[23] Larson, A. C.; Von Dreele, R.B.; *Generalized Structure Analysis System (GSAS)*; Los Alamos National Laborator Report LAUR 86-748, 1994.

(24)[24] Blaha, P.; Schwarz, K.; Madsen, G. K. H.; Kvasnicka, D.; Luitz, J., **WIEN2k**, An Augmented Plane Wave + Local Orbitals Program for Calculating Crystal Properties (Karlheinz Schwarz, Techn. Universitat Wien, Austria), 2001, ISBN 3-9501031-2.

[25] Galasso, F. S.; *Structure, Properties and Preparation of Perovskite-Type compounds*; Pergamon, London, 1969.

(1)[26] Westerburg, W.; Lang, O.; Ritter, C.; Felser, C.; Tremel, W.; Jakob, G. *Solid State Commun*. 2002, **122**, 201.

[27] Shannon, R. D. *Acta Crystallogr. A* 1976, **32**, 751.

[28] Amow, G.; Greedan, J. E.; Ritter, C. *J. Solid State Chem*. 1998, **141**, 262.

[29] Azad, A. K.; Ivanov, S.; Eriksson, S. –G.; Rundlöf, H.; Eriksen, J.; Mathieu, R.; Svedlindh, P. *J. Magn. Magn. Mater*. 2001, **237**, 124.

[30] Crocombette, J. P., Pollak, M.; Jollet, F.; Thromat, N.; Gautier-Soyer, M. *Phys. Rev. B* 1995, **52**, 3143.

[31] Gautier-Soyer, M. *J. Eur. Cer. Soc*. 1998, **18**, 2253.

[32] Woodward, P. M. *Acta Crystallogr., Sect.* B 1997, 53, 32.

[33] Chan, T. S.; Liu, R. S.; Guo, G. Y.; Huang, C. Y, *Int. J. Mod. Phys. B* (in press).

[34] Chan, T. S.; Liu, R. S.; Guo, G. Y.; Hu, S. F.; Lin, J. G.; Chen, J. M,; Ching-Ray. Chang, *Submitted to Chem. Mater*.

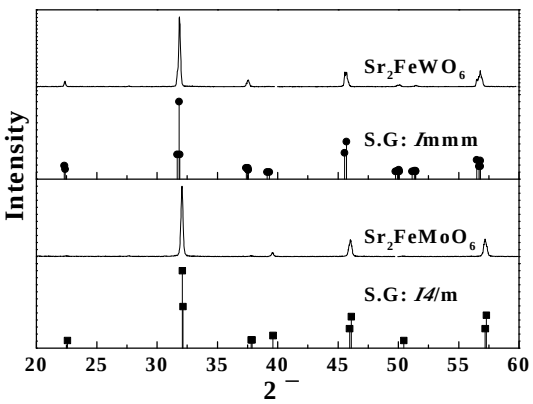

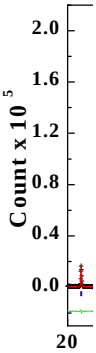

Fig. 1. XRD patterns of Sr_2FeMoO_6 indexed in a tetragonal unit cell (*I4/m*) and Sr_2FeWO_6 indexed in a orthorhombic unit cell (*Immm*).

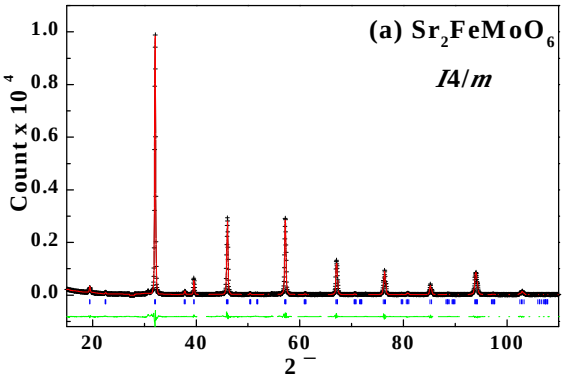

Fig. 2. Rietveld fits to powder XRD data of Sr_2FeMO_6 (M = Mo, W) with (a) Sr_2FeMoO_6 ; space group *I4/m* and (b) Sr_2FeWO_6 space group *Immm*, at 300K. Observed (crosses) and calculated (solid line) intensities are shown with the difference at the bottom.

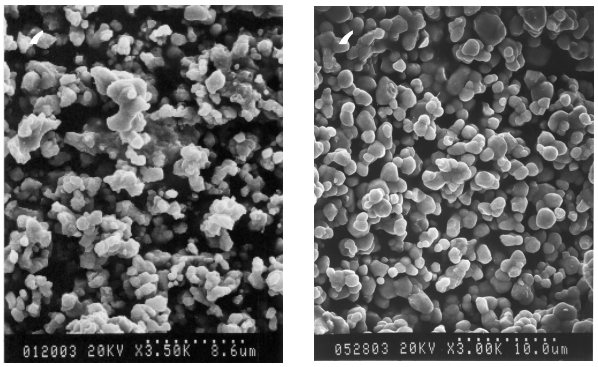

Fig. 3. Scanning electron micrograph of Sr_2FeMO_6 (M = Mo, W) with (a) Sr_2FeMoO_6 and (b) Sr_2FeWO_6.

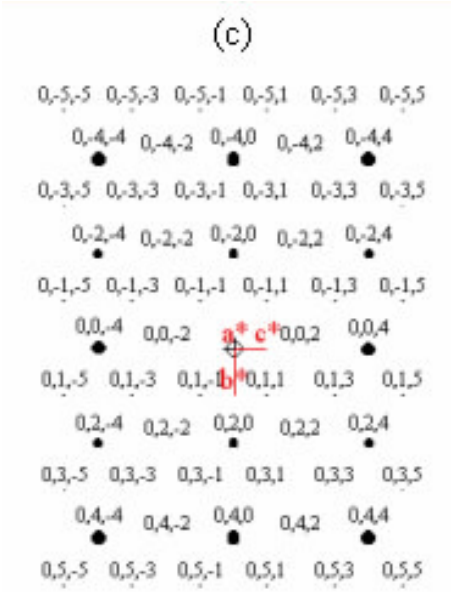

Fig. 4. (a) ED pattern and (b) HRTEM lattice image along the [100] direction of Sr_2FeWO_6 sample. (c) Simulated pattern along the zone axis [100].

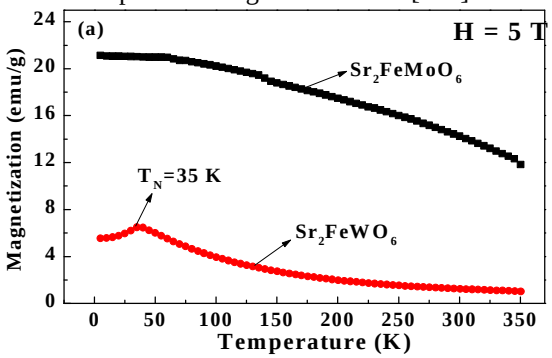

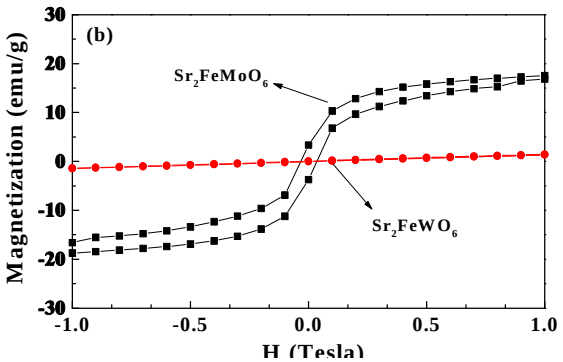

Fig. 5. (a) Temperature dependence of high-field (H = 5 T) magnetization of Sr_2FeMO_6 (M = Mo, W) (b) The magnetization hysteresis curves (*M* vs. *H*) recorded at T =5 K of Sr_2FeMO_6 (M = Mo, W).

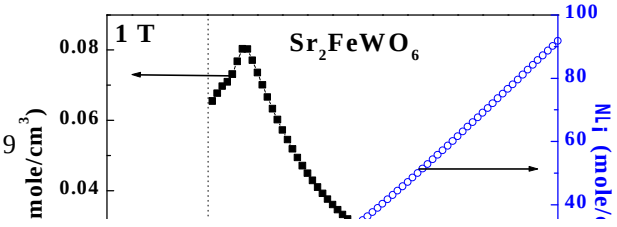

Fig. 6. Magnetic susceptibility (÷) and Curie-Weiss plot for Sr_2FeWO_6 in the temperature from 5 K to 350 K.

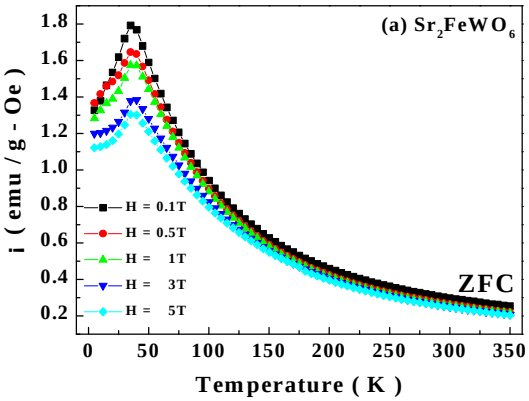

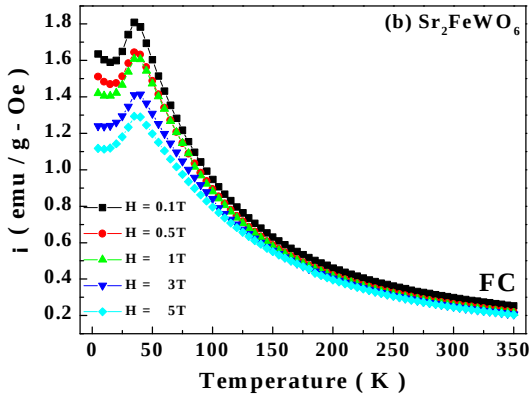

Fig. 7. Magnetic susceptibility (÷) vs. temperature in (a) zero-field cooled (ZFC) and (b) field cooled (FC) of Sr_2FeWO_6 measured with the applied field H =0.1, 0.5, 1, 3 and 5 T.

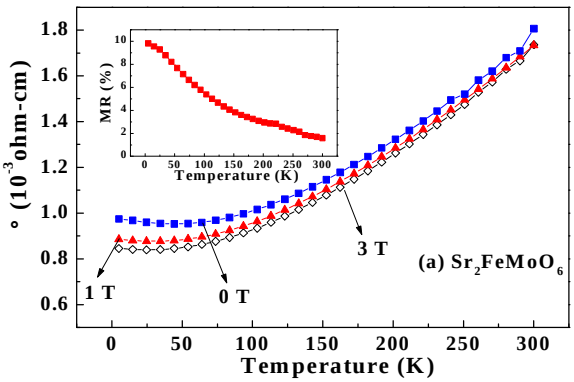

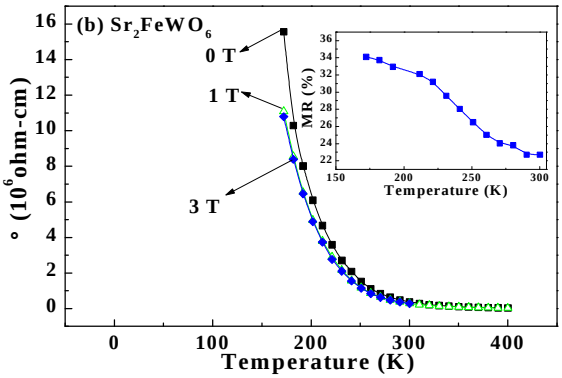

Fig. 8. Temperature dependence of resistivity at a magnetic field of 0 T, 1 T and 3 T of Sr_2FeMO_6 (M = Mo, W) with (a) Sr_2FeMoO_6 and (b) Sr_2FeWO_6. (b) Plot of MR% against temperature of Sr_2FeMO_6 (M = Mo, W) is also given in the inset.

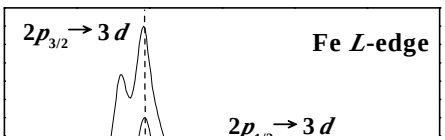

Fig. 9. Fe 2*p*-edge X-ray absorption near edge structure (XANES) spectra of Sr_2FeMoO_6 and Sr_2FeWO_6 along with of three standards, FeO, Fe_2O_3 and Fe_2O_3

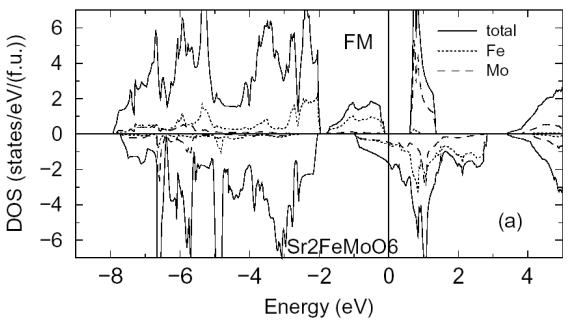

Fig. 10. The density of states (D.O.S) of (a) Sr_2FeMoO_6 and (b)(c) Sr_2FeWO_6.

附件)

員會補助專題研究計畫

利用化學控制合成新穎電子/離子作用氧化物及其特性分析(1/3)

出國研究心得報告

計畫編號：NSC 91－2113－M－002－044

出國期間：91 年 8 月 26 日至 91 年 8 月 28 日

出國人員：劉如熹　台灣大學化學系（計畫主持人）

中 華 民 國 九 十 二 年 六 月

會議經過:

2002 年第二次 IEEE 奈米技術會議(2002 2nd IEEE Conference on Nanotechnology；IEEE NANO' 2002)於八月二十六日至二十八日於美國華盛頓(Washington D.C.)之希爾頓飯店(Hilton Hotel)召開。會議由美國海軍研究所之 Clifford Lau 博士擔任一般主席(general chair)，而由芝加哥伊利諾大學之 George Uslenghi 教授擔任議程主席(program chair)。大會計收到約二百多篇論文，其中僅接受 190 篇之口頭(oral)論文發表，於為期三天的議程中計涵蓋下列主題：

-Phonons in nanostructures and nanodevices
-Nanofabrication, nanolithography, and growth and synthesis of nanostructures
-Atomic force microscopy, nano-scale manipulators and scanning tunneling microscopy
-Nanowire devices and applications
-Nanomagnetics
-The science and technology of nano and molecular electronics
-Nanotechnology: biological systems and applications
-Nanophotonics, optics in nanoscience, and optical diagnostics
-Nanoelectronics: MOS structures, molecular transistors, devices, components, and transport
-Nanometamatrerials
-Nanoelectronics
-Nanocrystalline structures and particles
-Molecule-based devices -quantum dots and forces on nanoparticles: applications and properties
-Assembly, patterning, and manipulation on the nanoscale
-Nanotechnology: institution, commercial, and manufacturing perspectives;

patent databases and analytical tools
-Nanotubes: devices, applications, processing and assembly
-Enviromental implications of nanotechnology
-Single-electron devices and systems

議程中第二天下午安排一 Panel Discussion，題目為：Grand Challenges in Nanoelectronics ，由各國專家先報告其對本主題之看法，再由聽眾提出問題共同討論，此種方式於一般國際會議例屬少見，但此種雙向溝通非常有助於對主題之瞭解。於會議中一般均同意奈米技術將由 2004 年之 90 奈米至 2016 年之 22 奈米發展之趨勢，但 2016 年後新的物理機制將被發展，而屆時亦有新的 scaling law 出現。至 2040 年單電子元件之技術將純熟，但其必符合為一穩定、可重複與低價且量產之生產率，於其時重要關鍵性產品將出現。一般預估未來元件與奈米電子相關產業之市場約為 6 億美元。

第二天傍晚大會安排一 Plenary talk，由普林斯頓大學之 Steven Y. Chou 教授演講，題目為： A Grand Challenge in Nanoelectronics ，其於演講中首先闡述各種新的元件，如 quantum effect devices、 single-electron devices、carbon nanotube devices，其並報告利用高分子具自組裝特性並配合轉印技術而提出新的奈米製程方法，其並預估未來奈米技術相關市場為: A trillions US Dollars Market。

於議程中值得參考之演講略述如下：

(1) 日本 NTT 公司之 Akira Fujiwara 博士報告題為：Nanotechnology Research in NTT ，其報告該公司於矽奈米元件及奈米光晶體(photonic crystal)之發展現況，其目標由奈米技術(nanotechnology；NT)進入量子資訊技術 (quantum information technology；QIT)，其並指出單電子電晶體因以單電子操作，故具極低之輸入能量(ultra-low power)，且因其非常小之體積，故具極大尺度之整合(Ultra-large scale integration)。最近該公司已發展出 3 nm 寬度直型及 Y 型單電子電晶體，並於室溫具庫倫阻斷效應。
(2) 日本 RIKEN 研究所之 Eiichi Maruyama 教授報告題為：Nanotechnology Research Promotion at RIKEN ，其報告該研究所自 1980 年即發展奈米技術相關之研究，目前正與工業界、學界及其他研究所成立整合型計畫，其乃欲發展奈米相關之生化、量測、資訊等技術。
(3) 澳洲之澳大利亞國立大學之 C. Jagadish 教授報告題為：Nanotechnology Research in Australia ，其報告中指出 Australian Research Council (ARC)於 2003 年計投入澳幣 1 仟 300 萬至 1 仟 500 萬元於奈米相關之研究，主要發展奈米材料。
(4) 台灣工研院電子所之之蔡銘進博士報告題為： Nanoelectronics Research at ERSO/ITRI，其報告該研究所未來將發展單電子電晶體(與荷蘭合作)，記憶及邏輯相關之奈米元件。
(5) 美國休士頓大學之 W. N. Hulsey III 博士報告題為：Patent Databases and Analytical Tools for Nanotechnology Research, Design and development ，其報告自 1925 年至 1995 年專利呈指數成長之趨勢，於未來奈米技術之發展世界各先進國均投入相當之財力，故對專利之爭取更是發展未來奈米相關之工業之決勝關鍵，其演講中亦提出如何利用專利查詢方法瞭解目前奈米技術之發展。
(6) 美國 Rice 大學之 Vicky Colvin 教授報告題為：Nanotechnology and the Enviroment ，其報告中指出奈米材料並非為一非活性行(inert) 材料，其進入我們生存之環境或人體將造成某種程度之危害，故呼籲發展奈米材料雖有所助益人類對更深入技術之產品之掌握，但亦會於此同時對其造成危害之評估亦漸形重要。

參加心得：

奈米技術之研究衍然已成為二十一世紀全世界科研之盛事，有鑑於此 IEEE 學會舉辦此第二次之國際性研討會，有助於全世界各國研究人員對奈米科技於電子相關技術與元件發展概況之瞭解。由會議中大家對奈米技術共同之認知為：(1)透過 bottom-up/top-down 接近之共同基礎技術，(2)具整合性(interdisciplinary)與(3)影響未來新元件與新功能產品之發展。透過對奈米技術之操控所產生之奈米結構元件將展現新機械、熱、電子、光子及量子等特性。於會議中本人發表題為: Growth of Nano-sized Copper Seed Layer on TiN and TaSiN by New Non-toxic Electroless Plating 之演講，此乃全世界首度於 TaSiN 之阻障層可利用無電極電鍍之方法成功第地成長銅之晶種層，本報告得到各國代表專家之好評，使其對我們實際於奈米半導體製程之發展有所認識，此外並與各國專家充分交換研究心得，獲益良多，於此感謝國科會之補助。

攜回資料:

大會議程及論文集(含光碟片)各一份。